

THE X-RAY TO MID-INFRARED RELATION OF AGN AT HIGH LUMINOSITY

DANIEL STERN¹

Accepted version – May 2015

ABSTRACT

The X-ray and mid-IR emission from active galactic nuclei (AGN) are strongly correlated. However, while various published parameterizations of this correlation are consistent with the low-redshift, local Seyfert galaxy population, extrapolations of these relations to high luminosity differ by an order of magnitude at $\nu L_\nu(6\ \mu\text{m}) \sim 10^{47}\ \text{erg s}^{-1}$. Using data from the *Wide-field Infrared Survey Explorer*, we determine the mid-IR luminosities of the most luminous quasars from the Sloan Digital Sky Survey and present a revised formulation of the X-ray to mid-IR relation of AGN which is appropriate from the Seyfert regime to the powerful quasar regime.

Subject headings: galaxies: active

1. INTRODUCTION

Several groups have investigated how the X-ray and mid-IR emission from active galactic nuclei (AGN) are correlated. Lutz et al. (2004) and Gandhi et al. (2009) investigated local samples of Seyfert galaxies, establishing this correlation at low luminosities. Fiore et al. (2009) investigated unobscured (or type-1) AGN at higher luminosities identified in the COSMOS and *Chandra* Deep Field-South (CDF-S) fields, while Lanzuisi et al. (2009) investigated obscured (or type-2) AGN at similar luminosities identified in *Spitzer* fields. However, while these various efforts have presented X-ray to mid-IR correlations that are largely consistent at low luminosity, extrapolation of these results to high luminosity differ by an order of magnitude at $\nu L_\nu(6\ \mu\text{m}) \sim 10^{47}\ \text{erg s}^{-1}$.

This can be particularly problematic for investigations into obscured, high-luminosity AGN. Obscuration will preferentially affect UV and (low-energy) X-ray emission, while the mid-IR emission is largely unaffected until the most extreme obscuring columns are attained ($A_V \sim 30$). Several investigations have therefore adopted the mid-IR luminosity of AGN as a robust indicator of the intrinsic AGN strength, and then used the relative luminosity at X-ray energies to measure the amount of obscuration (e.g., Fiore et al. 2008, 2009; Georgantopoulos et al. 2011; Luo et al. 2013; Lansbury et al. 2014; Rovilos et al. 2014; Stern et al. 2014). However, with substantial discrepancies between published intrinsic X-ray to mid-IR luminosity ratios for luminous quasars, this leads to uncertainties in such analyses.

Using data from the *Wide-field Infrared Survey Explorer* (*WISE*; Wright et al. 2010), we determine the mid-IR luminosities of a sample of extremely luminous unobscured quasars from Just et al. (2007), who reported on their X-ray properties. The sample consists of essentially all the most optically luminous quasars known at the time ($M_i \approx -29.3$ to -30.2). We supplement these data with published X-ray and mid-IR luminosities of sources at lower luminosities, including published high-resolution mid-IR imaging of nearby Seyfert galaxies observed with VLT which allow for robust separation of the nuclear emission from host galaxy emission. Combining these various data sets, we present a revised X-ray to mid-IR relation of AGN spanning from

low luminosity Seyfert galaxies to the most powerful quasars known. Throughout, we adopt the concordance cosmology, $\Omega_M = 0.3$, $\Omega_\Lambda = 0.7$ and $H_0 = 70\ \text{km s}^{-1}\ \text{Mpc}^{-1}$.

2. SAMPLES AND MID-IR LUMINOSITIES

This section describes several AGN samples with mid-IR and X-ray data publicly available, which we use to investigate the relation between AGN luminosities in these two energy ranges. A concern in such work is host galaxy contamination to the AGN luminosity. This is less problematic at higher energies as 0.5-10 keV X-ray luminosities above $3 \times 10^{42}\ \text{erg s}^{-1}$ are predominantly due to AGN, with only rare, extreme starbursts in the distant universe as exceptions (see review by Brandt & Alexander 2015). At mid-IR wavelengths, host galaxy contamination can be a larger concern, particularly for lower luminosity samples as the AGN becomes a minor contributor to the overall IR luminosity of a galaxy. For these lower luminosity sources, we rely on published work which separates the host and nuclear emission either through high-resolution imaging (Gandhi et al. 2009) or spectral decomposition (Lutz et al. 2004). At higher luminosities, entering into the quasar regime, host galaxy contamination becomes less of a concern. We adopt a traditional line at 2-10 keV X-ray luminosities of $10^{43}\ \text{erg s}^{-1}$ to identify quasars, with the caveat that mid-IR spectra of sources at these luminosities do sometimes show star-formation features, implying that a measurable fraction of the mid-IR emission is not related to the central engine.

Regarding that latter point, Murphy et al. (2009) and Fadda et al. (2010) present deep *Spitzer* mid-IR spectroscopy of IR-selected galaxies from the GOODS-N and GOODS-S fields, respectively. Fadda et al. (2010) finds that galaxies with 2-8 keV luminosities $\gtrsim 10^{44}\ \text{erg s}^{-1}$ are strongly AGN dominated in the mid-IR. Murphy et al. (2009) includes three galaxies with 2-8 keV luminosities between $10^{43}\ \text{erg s}^{-1}$ and $5 \times 10^{43}\ \text{erg s}^{-1}$, all three of which show star formation contributions to the mid-IR luminosity as evidenced by polycyclic aromatic hydrocarbon (PAH) features. Based on mid-IR spectral modeling, Murphy et al. (2009) reports mid-IR AGN fractions of $\sim 50\%$ for all three galaxies. While this is somewhat a concern, we note that the majority of the high luminosity sources in our analysis detailed below are considerably more luminous, where such contributions should be less. Finally, we emphasize that the above work on mid-IR spectra were from IR-selected samples, not X-ray or optically selected samples, so would be biased towards sources where

¹ Jet Propulsion Laboratory, California Institute of Technology, 4800 Oak Grove Drive, Mail Stop 169-221, Pasadena, CA 91109, USA [e-mail: daniel.k.stern@jpl.nasa.gov]

mid-IR emission from star formation was strongest.

2.1. High Luminosity Sample

Just et al. (2007) reports on the X-ray properties of the most luminous quasars from the Sloan Digital Sky Survey (SDSS) using a mixture of dedicated *Chandra* observations and archival data from *Chandra*, *XMM-Newton* and *ROSAT*. The core sample are the 32 quasars in the SDSS Data Release 3 (DR3) quasar catalog (Schneider et al. 2005) with $M_i < -29.28$. The quasars are in the redshift range $1.5 < z < 4.6$, and the sample is supplemented with two luminous quasars in the DR3 survey area that were missed by SDSS.

In our analysis, we exclude several of the sources from the core sample (Table 1). First, we exclude known gravitationally lensed quasars, for which the measured luminosities are not representative of the intrinsic values. We exclude broad absorption line (BAL) quasars, which are known to often exhibit suppressed X-ray emission (e.g., Gallagher et al. 2002; Luo et al. 2013, 2014; Teng et al. 2014). Following Just et al. (2007), we exclude the anomalously X-ray weak quasar SDSS J1521+5202 which lacks Ly α emission; SDSS J1521+5202 instead exhibits strong Ly α absorption, suggestive of absorbing material along the line-of-sight. We also exclude SDSS J1350+5716 and SDSS J1421+4633, which only have two and four *Chandra* counts, respectively. The remaining *Chandra*-observed sources in our sample have between 10 and 348 counts in the typically 4 ks *Chandra* observations, with a median value of 41 counts. Only two sources have less than 20 counts (SDSS J1438+4314 – 10 counts; SDSS J0209–0005 – 18 counts).

Table 1 presents the rest-frame 2–10 keV X-ray luminosities of the Just et al. (2007) sample. The values, which come directly from that work, have been corrected for the Galactic absorption to each source, as well as the quantum efficiency decay of *Chandra* at low energies. The fluxes were calculated using PIMMS, assuming a power-law model with $\Gamma = 2.0$, which is a typical photon index for luminous AGN (e.g., Reeves & Turner 2000; Vignali et al. 2005). This assumes the intrinsic X-ray absorption to be negligible for these luminous, broad-lined quasars. This assumption is supported by the fact that the observed band ratios presented in Just et al. (2007) are consistent with $\Gamma = 2.0$ for most of the culled sample (e.g., $\Gamma = 2.0$ is within the 1σ range for 16 of the 24 sources and within the 2σ range for 22 sources). The X-ray spectral fitting finds Γ significantly different from 2.0 for only two of the included sources, SDSS J1614+4704 ($\Gamma = 1.5 \pm 0.2$) and SDSS J2123–0050 ($\Gamma > 2.1$), but our results are essentially unchanged whether or not we include these two sources.

We determine the rest-frame $6\mu\text{m}$ luminosities for this sample of luminous quasars using *WISE*. We exclude SDSS J1733+5400 for which the mid-IR photometry is corrupted from the scattered light halo of a nearby bright source (ccflag = hHHH). The remaining 23 core sample quasars have robust mid-IR photometry from *WISE*. For the $12\mu\text{m}$ channel of *WISE* (*W3*), the signal-to-noise ratio of the core sample ranges from 9.9 to 58.4, with a median value of $\langle SNR_{W3} \rangle = 29.8$. For the $22\mu\text{m}$ channel of *WISE* (*W4*), the corresponding range is 5.0 to 26.4, with a median value of $\langle SNR_{W4} \rangle = 10.5$. For redshifts $z < 3.7$, which includes all but the three highest redshift quasars in the core sample, rest-frame $6\mu\text{m}$ is within the *W3* to *W4* wavelength range. We therefore simply linearly interpolate (or extrapolate for the $z > 3.7$ quasars) the *W3* and *W4* photometry to determine the rest-frame $6\mu\text{m}$ luminosity, $\nu L_\nu(6\mu\text{m})$. Table 1 presents

Table 1
High luminosity sample.

SDSS ID	z	$\log \nu L_\nu(6\mu\text{m})$	$\log L_{2-10}$	Notes
J012156.04+144823.9	2.87	46.96	45.52	
J014516.59–094517.3	2.73	46.87	46.13	lensed
J020950.71–000506.4	2.85	47.16	45.24	
J073502.31+265911.4	1.97	47.02	45.08	
J075054.64+425219.2	1.90	46.92	45.16	
J080342.04+302254.6	2.03	46.51	45.32	
J081331.28+254503.0	1.51	47.20	45.68	lensed
J084401.95+050357.9	3.35	47.10	45.31	BAL
J090033.49+421546.8	3.29	47.14	45.97	
J094202.04+042244.5	3.28	46.79	45.59	
J095014.05+580136.5	3.96	47.05	45.55	
J100129.64+545438.0	1.76	46.65	45.11	
J101447.18+430030.1	3.13	47.05	45.38	
J110610.73+640009.6	2.20	47.09	45.65	
J111038.64+483115.6	2.96	47.26	45.30	
J121930.77+494052.3	2.70	47.02	45.79	
J123549.47+591027.0	2.82	46.73	45.37	
J123641.46+655442.0	3.39	47.10	45.35	
J135044.67+571642.8	2.91	46.48	44.31	excluded
J140747.22+645419.9	3.08	46.82	45.61	
J142123.98+463317.8	3.37	47.10	44.66	excluded
J142656.17+602550.8	3.19	47.46	45.44	
J143835.95+431459.2	4.61	47.21	45.31	
J144542.75+490248.9	3.88	46.89	46.01	
J152156.48+520238.4	2.19	47.04	43.95	excluded
J152553.89+513649.1	2.88	46.93	45.92	BAL
J161434.67+470420.0	1.86	46.96	45.63	
J162116.92–004250.8	3.70	47.12	45.82	
J170100.62+641209.0	2.74	47.25	45.40	
J173352.22+540030.5	3.43	46.52	45.56	excluded
J212329.46–005052.9	2.26	47.03	45.20	
J231324.45+003444.5	2.08	46.84	44.62	BAL

Note. — Luminosities are in units of erg s^{-1} . BAL indicates broad absorption line quasars, which, along with known gravitationally lensed quasars, are excluded in the analysis. See §2.1 for details on the other excluded sources. Luminosities are in the rest-frame, and 2–10 keV X-ray luminosities, from Just et al. (2007), are absorption-corrected.

luminous quasar sample with their redshifts, mid-IR luminosities and absorption-corrected, rest-frame 2–10 keV X-ray luminosities from Just et al. (2007). Figure 1 plots these rest-frame 2–10 keV luminosities against rest-frame $6\mu\text{m}$ luminosity, and Figure 2 plots the residuals of these points relative to the new X-ray to mid-IR relation derived in § 3.2.

In their analysis of the X-ray to optical properties of luminous quasars, Just et al. (2007) also include a complementary sample of $z \gtrsim 4$ quasars with $M_i \lesssim -29$ from outside the SDSS DR3 quasar region with available X-ray data. The vast majority of these sources are at such great distance that they are faint or undetected by *WISE* (e.g., $SNR_{W4} < 3$). We therefore do not include this sample in our analysis.

2.2. SEXSI Sample

The Serendipitous Extragalactic X-ray Source Identification (SEXSI) program surveyed 2–10 keV selected sources from more than 2 deg² identified serendipitously in several dozen extragalactic pointings by *Chandra* (Harrison et al. 2003; Eckart et al. 2005, 2006, 2010). Out of a total sample of 1034 sources, SEXSI obtained nearly 500 spectroscopic identifications of sources with intermediate hard X-ray fluxes, $S(2–10 \text{ keV}) \sim 10^{-13}$ to $10^{-15} \text{ erg cm}^{-2} \text{ s}^{-1}$. SEXSI complements the *Chandra* Deep Fields, which reach depths more than an order magnitude fainter, but cover a total area of less than 0.2 deg². In Figure 1 we plot the X-ray and mid-IR properties of a subset of SEXSI sources from Eckart et al. (2010), which reported on *Spitzer* mid-IR follow-up of ap-

Table 2
SEXSI sample.

SEXSI ID	z	$\log \nu L_\nu(6\mu\text{m})$	$\log L_{2-10}$
J084854.4+445149	1.03	44.50	43.89
J084858.0+445434	0.57	44.68	43.87
J091027.0+542054	1.64	44.77	44.38
J091028.9+541523	0.65	43.78	43.67
J091041.4+541945	0.79	44.03	43.88
J091059.4+541715	1.86	44.88	44.61
J091100.2+542540	1.89	45.57	44.71
J133810.9+293119	2.03	45.53	44.77
J171614.4+671344	1.13	44.46	43.93
J171635.5+671626	0.50	43.49	43.37
J171638.0+671155	1.33	44.15	43.98
J224716.9+033432	3.82	45.96	45.71
J224731.6+033550	1.00	44.57	43.87

Note. — Luminosities are in the rest-frame, in units of erg s^{-1} . X-ray luminosities are from Eckart et al. (2010), corrected for intrinsic absorption reported in that work and adjusted for the different cosmology adopted here. See §2.2 for details.

proximately one-third of the SEXSI survey fields. Specifically, Eckart et al. (2010) provides mid-IR photometry for 290 of the 1034 SEXSI sources. We only plot sources whose optical spectra are classified as broad-lined AGN (65 of the 290 sources in Eckart et al. 2010). Since we are interested in rest-frame $6\mu\text{m}$ luminosities, we require sources have good photometry at both 8 and $24\mu\text{m}$ ($\text{flag} = 1$ in Eckart et al. 2010, implying robust counterparts with $\geq 5\sigma$ detections, unaffected by nearby bright sources), from which we interpolate the mid-IR fluxes to determine luminosities at rest-frame $6\mu\text{m}$. This further reduces the sample to 25 targets. In order to avoid low-luminosity sources for which the mid-IR photometry might be contaminated by host galaxy light, we require $L(2-10\text{ keV}) \geq 10^{43} \text{ erg s}^{-1}$, which eliminates two sources. We also require robust hard band detections, with $\text{SNR}_{2-10} \geq 3$, which eliminates seven additional sources, leaving a sample of 16 sources.

The plotted X-ray luminosities are based on the Galactic absorption-corrected 2-10 keV luminosities reported in Eckart et al. (2010), adjusted to both account for the slightly different cosmology adopted in that work as well as to correct for the intrinsic absorption measured in that work based on X-ray spectral fitting with XSPEC. We assume an intrinsic power-law X-ray spectrum with $\Gamma = 1.9$, as typical of quasars at this luminosity, to derive this final correction factor. As a final clean-up of the sample, we drop the three most heavily obscured sources based on the spectral modeling, all sources with $N_{\text{H}} \sim 10^{23} \text{ cm}^{-2}$, corresponding to correction factors $> 65\%$. The median neutral column of the remaining 13 sources is $\langle N_{\text{H}} \rangle = 2.5 \times 10^{21} \text{ cm}^{-2}$, and the median obscuration correction factor is 2.4%. All remaining sources have correction factors $< 15\%$, and 9 of the 13 have correction factors $< 5\%$. In the end, this leaves a total sample of 13 broad-lined SEXSI quasars with robust photometry at both X-ray and mid-IR energies (see Table 2). As expected, the broad-lined AGN in SEXSI are at lower luminosities than the extreme sources from Just et al. (2007).

2.3. SDSS DR5 Sample

Young et al. (2009) cross-matched the SDSS Data Release 5 (DR5) quasar catalog with the *XMM-Newton* public archive. A total of 792 quasars were matched, and Young et al. (2009) provide basic X-ray spectral fits for each source. For our anal-

ysis, we again exclude BAL quasars, and we only consider sources with $\geq 6\sigma$ X-ray detections that were best fit with a single, non-absorbed power-law model. For all such sources, Young et al. (2009) also fit an absorbed power-law model and provide the 90% upper limit to the intrinsic absorption, N_{H} . In order to avoid possibly obscured quasars, we require that the value of that parameter be less than 10^{21} cm^{-2} such that intrinsic absorption is negligible at rest-frame 2-10 keV. Similar to the SEXSI sample, we also require $L(2-10\text{ keV}) \geq 10^{43} \text{ erg s}^{-1}$ in order to avoid low-luminosity systems which might have more host galaxy contamination. We then cross-matched this subset of 441 quasars to the *WISE* archive, restricting our analysis to sources detected with robust, $\geq 5\sigma$ detections at both $12\mu\text{m}$ (78% of the sample) and $22\mu\text{m}$ (28% of the sample), as well as clean *WISE* photometry ($\text{ccflag} = 0000$). This requirement of robust mid-IR detections might introduce concerns with a bias towards high mid-IR emission quasars. However, the similar location of the SDSS DR5 quasars in Figure 1 to the SEXSI quasars of comparable X-ray luminosity but significantly deeper mid-IR data suggests this is not the case. Instead, the robust $22\mu\text{m}$ detections essentially biases the sample to lower redshift. Whereas the initial subset of 441 quasars has a median redshift $\langle z \rangle = 1.705$, the final, conservative sample of 90 SDSS DR5 quasars with robust X-ray and mid-IR detections, plotted in Figure 1 and listed in Table 3, has a median redshift of $\langle z \rangle = 0.618$. This plotted sample bridges the high luminosity quasars discussed in §2.1 and the local, low-luminosity samples discussed next in §2.4.

As a back-of-the-envelope exercise, we use the large, mid-luminosity SDSS quasar sample to investigate whether star formation contamination to the mid-IR luminosities could be impacting our results. *Herschel* studies show that AGN, on average, have similar star formation rates to massive ‘main sequence’ galaxies at similar redshift (e.g., Mullaney et al. 2012; Santini et al. 2012; Rosario et al. 2013). We therefore use the specific star formation rate of main sequence galaxies as a function of redshift determined by Elbaz et al. (2011), and assume host galaxy masses of $\log(M/M_{\odot}) = 10.5$ in order to derive typical star formation rates for the SDSS quasars. We then adopt the Rieke et al. (2009) conversion between star formation rate and $24\mu\text{m}$ luminosity. Based on the empirical star-forming galaxy templates of Assef et al. (2010), we shift these $24\mu\text{m}$ luminosities downwards by a factor of 1.5 to determine the estimated star-formation-related $6\mu\text{m}$ luminosities for the quasars in our sample. We then compare this to the observed $6\mu\text{m}$ luminosities. We find that the $6\mu\text{m}$ luminosities are strongly dominated by the AGN, with star formation accounting for just 1-2% of the observed $6\mu\text{m}$ luminosities, on average. In only one quasar does the inferred star formation contribute more than 50% of the observed $6\mu\text{m}$ luminosity, and in only three quasars does the inferred star formation contribute more than 33% of the observed $6\mu\text{m}$ luminosity. Assuming the above assumptions are valid, i.e., that the SDSS DR5 subsample of quasars are hosted by massive, main sequence galaxies, we therefore conclude that star formation contamination will, on average, have a negligible contribution to the $6\mu\text{m}$ luminosities of the quasars in our sample and not affect the final X-ray to mid-IR relation derived below.

2.4. Low Luminosity Samples

Horst et al. (2008) and Gandhi et al. (2009) report on near-diffraction-limited $12\mu\text{m}$ imaging of local Seyfert galaxies obtained with the VLT Imager and Spectrometer for the mid-

Table 3
SDSS DR5 sample.

SDSS ID	z	$\log \nu L_\nu(6\mu\text{m})$	$\log L_{2-10}$
J020011.52-093126.1	0.360	44.21	44.20
J020118.67-091935.7	0.661	45.24	44.46
J023402.08-084314.6	1.264	45.73	44.62
J074020.22+311841.2	0.296	43.80	43.48
J080608.13+244421.0	0.358	44.45	43.96
J080711.01+390419.7	0.369	44.21	44.16
J081422.12+514839.4	0.377	44.72	44.37
J082257.55+404149.7	0.865	45.84	44.88
J091029.02+542719.0	0.526	44.59	44.21
J091301.03+525928.9	1.377	46.65	45.88

Note. — Luminosities are in the rest-frame, in units of erg s^{-1} . X-ray luminosities are from Young et al. (2009). This table is published in its entirety in the electronic edition of ApJ; a portion is shown here for guidance regarding its form and content.

IR (VISIR; Lagage et al. 2004). The high spatial resolution allows them to measure the mid-IR luminosities of the galactic nuclei with minimal contamination from star formation in the outer galaxy. They also provide the intrinsic 2-10 keV luminosities for their sample with corrections applied for non-nuclear components, obscuration, and the modest redshift effects necessary for this local sample. In our study, we exclude the Compton-thick sources flagged in Gandhi et al. (2009) for which the intrinsic X-ray luminosities are more model dependent. We also exclude LINERS and sources without well-determined mid-IR and 2-10 keV X-ray luminosities. This leaves a final sample of 26 local galaxies with $\nu L_\nu(6\mu\text{m}) \lesssim 10^{45} \text{ erg s}^{-1}$. For the low redshifts of the sample considered here, the slightly different cosmology adopted by Gandhi et al. (2009) has negligible effect on our analysis.

The luminosities obtained for the local sample are at $12\mu\text{m}$, while we require rest-frame luminosities at $6\mu\text{m}$ to allow comparison with the high luminosity samples. Based on the empirical AGN template of Assef et al. (2010), this requires shifting the $12\mu\text{m}$ luminosities downwards by 5%. Figure 1 presents the X-ray luminosities plotted against mid-IR luminosity for the local sample.

2.5. *NuSTAR* Sample

Figure 1 also shows seven unbeamed X-ray sources identified from the *Nuclear Spectroscopic Telescope Array* (*NuSTAR*; Harrison et al. 2013) serendipitous survey (Alexander et al. 2013), as well as a *NuSTAR*-detected source at $z \sim 2$ in the *Chandra* Deep Field-South (Del Moro et al. 2014). These unobscured or only somewhat obscured (i.e., Compton-thin; $N_{\text{H}} < 1.5 \times 10^{24} \text{ cm}^{-2}$) sources all reside within the locus of broad-lined AGN in the X-ray to mid-IR plane.

Figure 1 also shows several heavily obscured sources studied by *NuSTAR* as purple asterisks. These sources are candidate Compton-thick AGN ($N_{\text{H}} \geq 1.5 \times 10^{24} \text{ cm}^{-2}$). At high luminosity ($\nu L_\nu(6\mu\text{m}) \sim 10^{47} \text{ erg s}^{-1}$), we show three *WISE*-selected sources at $z \sim 2$ reported in Stern et al. (2014); only one of the sources is detected in the rest-frame 2-10 keV band. At lower luminosity, we show three SDSS type-2 AGN discussed in Lansbury et al. (2014), one of which is undetected at X-ray energies. We also include the local luminous AGN Mrk 34, reported in Gandhi et al. (2014); this is the *NuSTAR* source with the lowest X-ray luminosity, $L(2-10 \text{ keV}) = 10^{42} \text{ erg s}^{-1}$. The *NuSTAR* heavily obscured

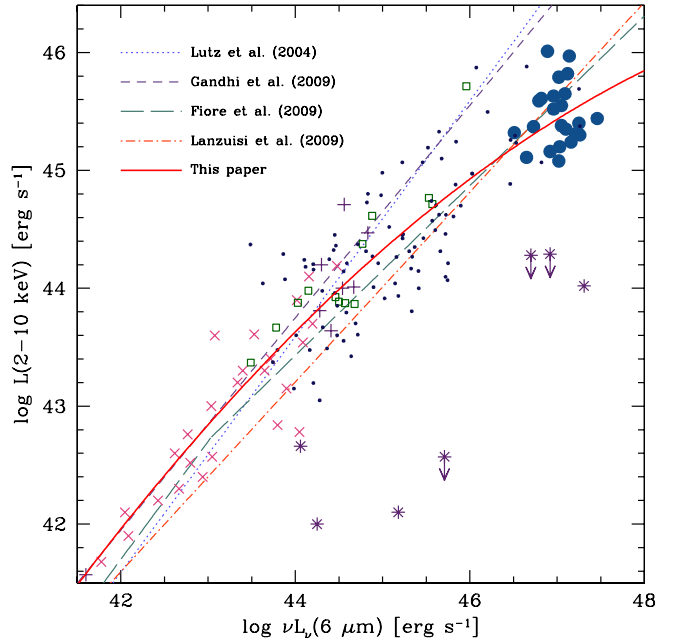


Figure 1. Rest-frame 2-10 keV X-ray luminosity against rest-frame $6\mu\text{m}$ luminosity for a sample of AGN with four published relations plotted (as indicated), as well as our new derivation of the X-ray to mid-IR relation (solid red). Large solid blue circles show luminous quasars from Just et al. (2007). Open green squares show broad-lined AGN from the SEXSI survey Eckart et al. (2010). Purple plus signs show Compton-thin AGN identified by *NuSTAR* (Alexander et al. 2013; Del Moro et al. 2014), while purple asterisks show candidate Compton-thick AGN studied by *NuSTAR* (Gandhi et al. 2014; Lansbury et al. 2014; Stern et al. 2014, see text for details). Small blue dots show quasars from SDSS DR5 with X-ray data reported in Young et al. (2009). Red crosses show local Seyfert galaxies from Horst et al. (2008) and Gandhi et al. (2009).

sources all reside below the X-ray to mid-IR relation of unobscured sources, illustrating how multi-wavelength surveys provide a powerful means of identifying heavily obscured AGN.

3. THE X-RAY TO MID-IR RELATION

3.1. Literature Relations

Several groups have previously published the X-ray to mid-IR correlation for AGN samples. Using spectral decomposition, Lutz et al. (2004) separated the nuclear component from the host galaxy in low resolution spectra of 71 local Seyfert galaxies observed with the *Infrared Space Observatory* (*ISO*). The median distance of their sources ranges from 50 to 100 Mpc (Seyfert 2 and Seyfert 1 galaxies, respectively). Figure 1 presents the correlation between mid-IR luminosity and absorption-corrected hard (2-10 keV) X-ray luminosity reported by Lutz et al. (2004) based on their sample.

Rather than using spectral decomposition to separate mid-IR nuclear emission from contaminating host galaxy emission, Gandhi et al. (2009) reports on high-resolution imaging obtained with VLT/VISIR to separate the nuclear and host galaxy contributions to the mid-IR emission of local AGN. Based on their cleaned sample of less obscured local AGN observed with VLT/VISIR, Gandhi et al. (2009) derived the relation shown in Figure 1. The consistency with the results of Lutz et al. (2004) are reassuring given the very different approaches. However, both samples had few sources with quasar-level X-ray luminosities, $L(2-10 \text{ keV}) > 10^{44} \text{ erg s}^{-1}$, and thus were forced to derive a relation with data over a lim-

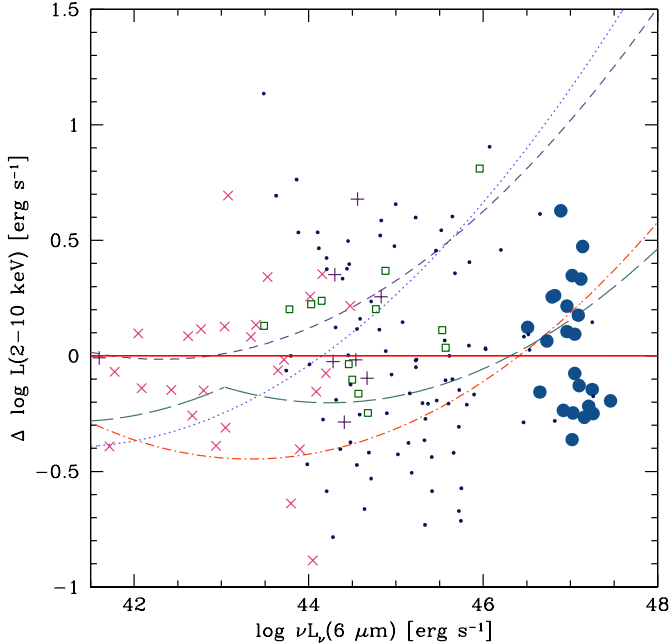


Figure 2. Difference between rest-frame 2-10 keV X-ray luminosity and the value predicted by the relation presented herein, plotted against rest-frame $6\mu\text{m}$ luminosity. Symbols and published relations are plotted as per Figure 1.

ited dynamic range, spanning approximately three decades in mid-IR luminosity. As clearly seen in Figure 1, these local relations do a poor job of predicting the mid-IR luminosities of the most luminous quasars, underpredicting the expected mid-IR luminosity of quasars with $L(2-10\text{ keV}) \gtrsim 10^{45}\text{ erg s}^{-1}$ by approximately an order of magnitude, or, alternatively, overpredicting the X-ray luminosities of quasars with $\nu L_\nu(6\mu\text{m}) \sim 10^{47}\text{ erg s}^{-1}$ by an order of magnitude.

Fiore et al. (2009) present the X-ray to mid-IR correlation based on a large sample of X-ray-selected type-1 AGN in the COSMOS and CDF-S fields using deep *Chandra* and *Spitzer* observations. By considering a sample of sources that reaches into the quasar regime, the Fiore et al. (2009) relation does a much better job at determining the X-ray to mid-IR ratio of luminous AGN. However, there is a systematic problem with the mid-IR luminosities of the lowest luminosity AGN being high, most likely due to host galaxy contamination within the *Spitzer* beam.

Lanzuisi et al. (2009) present an X-ray study of a sample of 44 mid-IR bright ($F_{24\mu\text{m}} > 1.3\text{ mJy}$) objects with extreme mid-IR-to-optical flux ratios ($F_{24\mu\text{m}}/F_R > 2000$) selected from an area of $\sim 6\text{ deg}^2$ of the $\sim 50\text{ deg}^2$ *Spitzer* Wide-area InfraRed Extragalactic (SWIRE; Lonsdale et al. 2003) survey with *Chandra* or *XMM-Newton* coverage. By selection, the sample is biased towards obscured AGN, and their X-ray to mid-IR correlation, presented in Figure 1, was derived from the SWIRE sample as well as additional Type 2 quasars from the literature, where the intrinsic X-ray luminosities were derived from X-ray spectral fitting. Perhaps unsurprising given the mid-IR selection bias to this sample, the Lanzuisi et al. (2009) relation is slightly offset towards decreased X-ray luminosity (or increased mid-IR luminosity) relative to the other relations plotted in Figure 1.

3.2. New Relation

We derive a new X-ray to mid-IR relation using the data sets from §2, which span accurate measurements of these quantities from low luminosity (§2.4) to high luminosity (§2.1). The sample also includes several AGN samples of intermediate luminosity. Doing a least-square polynomial fit to the data, we derive

$$\log L(2-10\text{ keV}) = 40.981 + 1.024x - 0.047x^2,$$

where $L(2-10\text{ keV})$ is in units of erg s^{-1} and $x \equiv \log(\nu L_\nu(6\mu\text{m})/10^{41}\text{ erg s}^{-1})$. If we were to require the non-local samples to have X-ray luminosities $\log L(2-10\text{ keV}) > 5 \times 10^{43}\text{ erg s}^{-1}$ so as to avoid sources with possible host galaxy contributions to their mid-IR emission, the relation would be essentially unchanged (changes < 0.2 dex; i.e., smaller than the dispersion in the relation shown in Figure 2) over the range of interest.

Several prior analyses have considered how the optical and X-ray luminosities of AGN scale over a wide range of AGN power (e.g., Strateva et al. 2005; Steffen et al. 2006). Such relations are typically discussed with reference to the parameter α_{ox} , defined by Tananbaum et al. (1979) as the slope of a nominal power law connecting the rest-frame 2500 Å and 2 keV monochromatic luminosities, $\alpha_{\text{ox}} \equiv 0.3838 \log(L_{2\text{keV}}/L_{2500\text{Å}})$. For unobscured AGN, α_{ox} compares the emission power coming from the AGN accretion disk (at rest-frame 2500 Å) relative to the emission power at rest-frame 2 keV, which is believed to originate from Compton up-scattering of accretion disk photons by hot coronal gas of unknown geometry or disk-covering fraction. Studies show that as 2500 Å accretion disk luminosity increases, the luminosity increases less dramatically at X-ray energies. The α_{ox} parameter thus probes the balance between accretion disks and their coronae, and provides a quantitative constraint on physical models of the structure and physics of AGN nuclear regions. The scatter in α_{ox} is considerable, corresponding to a factor of ~ 3 range of X-ray luminosities observed for sources at a given UV luminosity. Though some of this scatter is likely due to non-simultaneous observations at the two wavelengths, studies show that most of the scatter is actually intrinsic (e.g. Vagnetti et al. 2010; Gibson & Brandt 2012). Jin et al. (2012) show that α_{ox} is not correlated with black hole mass, but is somewhat correlated with Eddington ratio (see also Lusso et al. 2010). Steffen et al. (2006) reports that there is no significant evolution of α_{ox} with redshift.

We find a similar behavior here: as the mid-IR luminosity increases, the luminosity increases less dramatically at X-ray energies. AGN mid-IR emission is generally believed to be primarily due to thermal radiation from a torus reprocessing accretion disk emission. Previous results have shown that the mid-IR to bolometric luminosity of quasars, $L_{\text{MIR}}/L_{\text{bol}}$, decreases with increasing L_{bol} , an effect which is generally ascribed to the so-called receding torus model (e.g. Lawrence 1991; Simpson 2005; Assef et al. 2013): if the scale height of the torus is independent of the radial size of the torus, but the inner radius of the torus increases with increasing AGN luminosity, then the torus effectively covers a smaller solid angle for more luminous AGN. Thus, more luminous quasars are less likely to be seen as obscured, and will also have relatively diminished thermal IR emission from the obscuring torus. On the much smaller coronal scale, we also see a trend of decreasing L_X/L_{bol} with increasing L_{bol} . Therefore, L_X/L_{MIR} reflects the competition of physics occurring on very different size scales, from the sub-parsec coronal scale, to the much

larger obscuring torus scale, though a detailed investigation and modeling of this, accounting for various selection effects such as non-simultaneous X-ray and mid-IR imaging, is beyond the scope of the present work.

In summary, we have derived a new X-ray to mid-IR relation for AGN which is appropriate for AGN across a large range of luminosity, from local Seyfert galaxies with $L(2-10 \text{ keV}) \sim 10^{42} \text{ erg s}^{-1}$ out to the most powerful quasars known, with $L(2-10 \text{ keV}) \sim 10^{46} \text{ erg s}^{-1}$. Previous explorations of this relation have generally emphasized either just local Seyfert galaxies or just typical quasars, and no previous analyses have considered the most luminous quasars. The result is that extrapolations of the previous relations differ widely in certain regimes, particularly at the tip of the luminosity scale. The revised X-ray to mid-IR relation for AGN will be beneficial for identifying and studying highly obscured AGN, which will have their X-ray emission preferentially suppressed relative to their mid-IR emission.

The author gratefully acknowledges communications and input from close collaborators on the *NuSTAR* and *WISE* science teams, particularly David Alexander, Neil Brandt, Peter Eisenhardt, Poshak Gandhi, Michael Koss, George Lansbury, and Ezequiel Treister. I am also grateful to the referee, whose suggestions have improved the paper. This publication makes use of data products from the *Wide-field Infrared Survey Explorer*, which is a joint project of the University of California, Los Angeles, and the Jet Propulsion Laboratory/California Institute of Technology, funded by the National Aeronautics and Space Administration. The author also acknowledges support from NASA through ADAP award 12-ADAP12-0109.

Facilities: Chandra, Spitzer, WISE, XMM-Newton

©2015 California Institute of Technology. Government sponsorship acknowledged.

REFERENCES

- Alexander, D. M., Stern, D., Del Moro, A., et al. 2013, *ApJ*, 773, 125
 Assef, R. J., Kochanek, C. S., Brodwin, M., et al. 2010, *ApJ*, 713, 970
 Assef, R. J., Stern, D., Kochanek, C. S., et al. 2013, *ApJ*, 772, 26
 Brandt, W. N. & Alexander, D. M. 2015, *A&A Rev*, 23, 1
 Cao, C., Xia, X. Y., Wu, H., Mao, S., Hao, C. N. & Deng, Z. G. 2008, *MNRAS*, 390, 336
 Del Moro, A., Mullaney, J. R., Alexander, D. M., et al. 2014, *ApJ*, 786, 16
 Eckart, M., Laird, E., Stern, D., Mao, P., Helfand, D., & Harrison, F. 2005, *ApJS*, 156, 35
 Eckart, M., McGreer, I., Stern, D., Harrison, F., & Helfand, D. 2010, *ApJ*, 708, 584
 Eckart, M., Stern, D., Helfand, D., Harrison, F., Mao, P., & Yost, S. 2006, *ApJS*, 165, 19
 Elbaz, D., Dickinson, M., Hwang, H.S., et al. 2011, *A&A*, 533, 119
 Fadda, D., Yan, L., Lagache, G., et al. 2010, *ApJ*, 719, 425
 Fiore, F., Grazian, A., Santini, P., et al. 2008, *ApJ*, 672, 94
 Fiore, F., Puccetti, S., Brusa, M., et al. 2009, *ApJ*, 693, 447
 Gallagher, S. C., Brandt, W. N., Chartas, G., & Garmire, G. P. 2002, *ApJ*, 567, 37
 Gandhi, P., Horst, H., Smette, A., et al. 2009, *A&A*, 502, 457
 Gandhi, P., Lansbury, G. B., Alexander, D. M., et al. 2014, *ApJ*, 792, 117
 Georgantopoulos, I., Rovilos, E., Akylas, A., et al. 2011, *A&A*, 534, 23
 Gibson, R. R. & Brandt, W. N. 2012, *ApJ*, 746, 54
 Harrison, F., Eckart, M., Mao, P., Helfand, D., & Stern, D. 2003, *ApJ*, 596, 944
 Harrison, F. A., Craig, W. W., Christensen, F. E., et al. 2013, *ApJ*, 770, 103
 Horst, H., Gandhi, P., Smette, A., & Duschl, W. J. 2008, *A&A*, 479, 389
 Jin, C., Ward, M., & Done, C. 2012, *MNRAS*, 425, 907
 Just, D., Brandt, W. N., Shemmer, O., Steffen, A. T., Schneider, D. P., Chartas, G., & Garmire, G. 2007, *ApJ*, 665, 1004
 Lagage, P. O., Pel, J. W., Authier, M., et al. 2004, *The Messenger*, 117, 12
 Lansbury, G. B., Alexander, D. M., Del Moro, A., et al. 2014, *ApJ*, 785, 17
 Lanzuisi, G., Piconelli, E., Fiore, F., Fergulio, C., Vignali, C., Salvato, M. & Gruppioni, C. 2009, *A&A*, 498, 67
 Lawrence, A. 1991, *MNRAS*, 252, 586
 Lonsdale, C. J., Smith, H. E., Rowan-Robinson, M., et al. 2003, *PASP*, 115, 897
 Lusso, E., Comastri, A., Vignali, C., et al. 2010, *A&A*, 512, 34
 Luo, B., Brandt, W. N., Alexander, D. M., et al. 2013, *ApJ*, 772, 125
 Luo, B., Brandt, W. N., Alexander, D. M., et al. 2014, *ApJ*, 794, 70
 Lutz, D., Maiolino, R., Spoon, H. W. W., & Moorwood, A. F. M. 2004, *A&A*, 418, 465
 Mullaney, J. R., Pannella, M., Daddi, E., et al. 2012, *ApJ*, 753, 30
 Murphy, E. J., Chary, R.-R., Alexander, D. M., et al. 2009, *ApJ*, 698, 1380
 Page, K. L., Reeves, J. N., O'Brien, P. T., & Turner, M. J. L. 2005, *MNRAS*, 364, 195
 Reeves, J. N., & Turner, M. J. L. 2000, *MNRAS*, 316, 234
 Rieke, G. H., Alonso-Herrero, A., Weiner, B. J., Perez-Gonzalez, P. G., Blaylock, M., Donley, J. L. & Marcillac, D. 2009, *ApJ*, 692, 556
 Rosario, D. J., Santini, P., Lutz, D., et al. 2013, *ApJ*, 771, 63
 Rovilos, E., Georgantopoulos, I., Akylas, A., et al. 2014, *MNRAS*, 438, 494
 Santini, P., Rosario, D. J., Shao, L., et al. 2012, *A&A*, 540, 109
 Schneider, D. P., Hall, P. B., Richards, G. T., et al. 2005, *AJ*, 130, 367
 Simpson, C. 2005, *MNRAS*, 360, 565
 Steffen, A. T., Strateva, I., Brandt, W. N., et al. 2006, *AJ*, 131, 2826
 Stern, D., Lansbury, G. B., Assef, R. J., et al. 2014, *ApJ*, 794, 102
 Strateva, I. V., Brandt, W. N., Schneider, D. P., Vanden Berk, D. G., & Vignali, C. 2005, *AJ*, 130, 387
 Tananbaum, H., Avni, Y., Branduardi, G., et al. 1979, *ApJ*, 234, L9
 Teng, S. H., Brandt, W. N., Harrison, F. A., et al. 2014, *ApJ*, 785, 19
 Vagnetti, F., Turriziani, S., Trevese, D., & Antonucci, M. 2010, *A&A*, 519, 17
 Vignali, C., Brandt, W. N., Schneider, D. P., & Kaspi, S. 2005, *AJ*, 129, 2519
 Wright, E. L., Eisenhardt, P. R. M., Mainzer, A. K., et al. 2010, *AJ*, 140, 1868
 Young, M., Elvis, M., & Risaliti, G. 2009, *ApJS*, 183, 17